To appear in: The Astronomical Journal
(July 2002 issue)

Exploring the full stellar population of the Upper Scorpius OB Association

Thomas Preibisch
Max-Planck-Institut für Radioastronomie, Auf dem Hügel 69, D–53121 Bonn, Germany

Anthony G.A. Brown
Sterrewacht Leiden, P.O. Box 9513, NL-2300 RA Leiden, The Netherlands

Terry Bridges
Anglo-Australian Observatory, P.O. Box 296, Epping NSW 1710, Australia

Eike Guenther
Thüringer Landessternwarte Tautenburg, Sternwarte 5, D–07778 Tautenburg, Germany

Hans Zinnecker
Astrophysikalisches Institut Potsdam, An der Sternwarte 16, D–14482 Potsdam, Germany

ABSTRACT

We investigate the stellar population and star formation history of the Upper Scorpius OB association, the most nearby region of recent massive star formation, over the full stellar mass range from $0.1\,M_\odot$ to $20\,M_\odot$. The first part of this paper describes an extension of our large spectroscopic survey (Preibisch et al. 2001) for low-mass pre-main sequence (PMS) stars in Upper Scorpius. Utilizing the multi-object spectrograph 2dF at the Anglo-Australian-Telescope, we obtained spectra of 469 stars with magnitudes $R = 12.5-18.0$ in a 6 square-degree area. Among these we find 68 new PMS stars, nearly all of them M-type stars, by their strong lithium absorption lines. The total area covered by our 2dF survey is now 9 square-degrees and contains 166 new PMS stars. Combining these results with our earlier investigation (Preibisch & Zinnecker 1999) yields a sample of 250 PMS stars in the mass range $\sim 0.1\,M_\odot$ to $\sim 2\,M_\odot$. The location of these stars in the HR diagram suggests a mean age of 5 Myr without a significant age spread.

In the second part of this paper, we also consider the population of 114 high-mass members identified in detailed Hipparcos studies. We construct a combined HR diagram for the 364 high- and low-mass members and find that the whole stellar population is very well characterized by a very narrow age distribution around 5 Myr. We estimate individual masses for all members and construct an empirical mass function covering the mass range from $0.1\,M_\odot$ up to $20\,M_\odot$. A power-law fit to the mass function gives a slope of $\alpha \sim -2.6$ above $\sim 2\,M_\odot$ and a much flatter slope ($\alpha \sim -0.9$) below $\sim 0.6\,M_\odot$. The initial mass function of Upper Sco is not identical, but within the errors consistent with recent determinations of the field initial mass function. There is certainly no deficit of low-mass stars in the Upper Sco OB association, but rather a small excess of low-mass stars. Our results on the stellar age distribution confirm earlier indications that the star formation process in Upper Sco was triggered, and support previous conjectures that the triggering event was a supernova shock-wave originating from the nearby Upper Centaurus Lupus association.

1. Introduction

The study of the low-mass ($M_\star \leq 2\,M_\odot$) stellar population in OB associations can give us important information on the nature of the star formation process. For many years star formation was supposed to be a bimodal process (e.g. Larson 1986; Shu & Lizano 1988) according to which high- and low-mass stars should form in totally different sites. However, in nearby OB associations it has been long established that low-mass stars can form alongside their high-mass siblings (e.g. Herbig 1962). If OB associations actually do form low-mass stars in numbers predicted by the field star mass function, then the galactic star formation would be dominated by these regions (Miller & Scalo 1979). However, the question of what quantities of low-mass stars are produced in OB associations is still open; there have been many indications that high-mass star forming regions (most notably starburst regions; see Leitherer 1998) contain much smaller numbers of low-mass stars than expected from the field IMF (see discussion in Zinnecker et al. 1993). Even in nearby OB associations the low-mass stellar content is still only poorly known, mainly because of the enormous observational effort to identify the widespread population of low-mass PMS stars among the many thousands of field stars.

The stellar initial mass function (IMF) is of utmost importance for any theory of star formation. While the theoretical expectation is that the IMF should vary systematically with the star formation environment, no really convincing evidence for IMF variations has yet been found (for recent reviews see Kroupa 2002; Scalo 1998). The open question here is, whether the IMF is truly universal, or whether the systematic differences are too small to be reliably detected in empirical IMF determinations. The reliability of many empirical IMF determinations is very limited. In studies of clusters or associations, contamination by background objects from the galactic field population is a big problem and the observational effort required to obtain a complete sample of members is huge. Many IMF studies are based on photometric data only; while this strategy rather easily provides a complete spatial coverage and allows one to work with large samples, photometry alone cannot give completely reliable membership information. Most studies with spectroscopically identified member samples, on the other hand, include only very small fractions of the total stellar population and are strongly affected by small number statistics and the necessity of using large extrapolation factors. Therefore, most studies dealing with OB associations have been restricted to estimating the number-ratio of low-mass versus high-mass members (see e.g. Walter et al. 1994).

During the last few years, the situation has improved considerably and allowed more detailed studies of a few selected regions (see e.g. Dolan & Mathieu 2001 for the case of the λ Orionis region). In particular, the Hipparcos measurements boosted our knowledge of the high-mass stellar content of many OB associations. In several nearby associations the Hipparcos data even allowed the complete identification of the high- and intermediate-mass stellar population (see de Zeeuw et al. 1999). At the opposite end of the mass spectrum, new and very powerful multiple-object spectrographs like 2dF at the Anglo-Australian Telescope (see Lewis et al. 2002) made it possible to perform large, and even more importantly, *unbiased* spectroscopic surveys for low-mass PMS members. The combination of these two advances makes studies of the complete stellar population in OB associations feasible, enabling us to study in detail the spatial and temporal relationships between high- and low-mass star formation, and to derive the IMF over the full mass range.

2. The Upper Scorpius OB association

The OB association nearest to the Sun is the Sco OB2 or Scorpius-Centaurus association. It consists of three subgroups, the youngest of which is Upper Scorpius, located at a distance of 145 pc (see Blaauw 1991; de Geus et al. 1989; Preibisch & Zinnecker 1999; de Zeeuw et al. 1999). In contrast to the nearby ρ Oph molecular cloud (see Wilking 1991), which is located in front of the south-eastern edge of Upper Sco and is well known for its strong star formation activity, the star formation process in Upper Sco is finished and there are neither dense molecular clouds nor deeply embedded young stellar objects. The association members show only very moderate extinctions ($A_V \lesssim 2$ mag).

Below and in the rest of the paper we will make a distinction between the high- and the low-mass stellar population. The former refers to stars of spectral types F and earlier ($M \gtrsim 2\,M_\odot$) whose membership of Upper Sco was established using Hipparcos data (De Zeeuw et al. 1999). The latter refers to G, K, and M stars in the mass range 0.1–2.0 $M_\odot$ for which membership was established from their PMS character (Preibisch & Zinnecker 1999; Preibisch et al. 2001). Note that the mass ranges of the two groups of stars overlap slightly.

2.1. Previous Results on the High-Mass Stellar Population

The most recent (and definitive) investigation of the membership of high-mass stars in Scorpius-Centaurus was carried out by De Zeeuw et al. (1999; Z99 hereafter). They used Hipparcos proper motions and parallaxes in conjunction with two moving group methods in order to accurately establish the stellar content of 12 nearby OB associations down to mid-F spectral type. In Upper Sco the membership of 1215 stars in the Hipparcos Catalogue was investigated, of which 120 were identified as genuine members. The spectral types of the members on the (pre-)main-sequence range from B0.5V to G5V, and there are some evolved stars with giant luminosity classes.

The kinematic members of Upper Sco cover an area of about 150 square-degrees on the sky. The large intrinsic size of the association suggests that the spread of individual stellar distances cannot be neglected. The projected diameter on the sky is $\sim 14°$ which at the distance of Upper Sco corresponds to ~ 35 pc. However, while the Hipparcos data allow the determination of a very accurate mean distance of 145 ± 2 pc for Upper Sco (Z99), the errors on the trigonometric parallaxes (~ 1 mas) are too large to resolve the internal spatial structure. The only conclusion that can be drawn directly from the Hipparcos parallaxes is that the line-of-sight depth of Upper Sco cannot be much larger than ~ 70 pc. This prompted de Bruijne (1999) to carry out a more detailed investigation of the Hipparcos members of Scorpius-Centaurus by performing a careful kinematic modeling of the proper motion and parallax data. He used a maximum likelihood scheme based on a generalized moving-cluster method to derive secular (or 'kinematically improved') parallaxes for the association members. He showed that the method is robust and that the secular parallaxes are a factor of ~ 2 more precise than the Hipparcos trigonometric parallaxes. The secular parallaxes for the members of Upper Sco show a much reduced line-of-sight dispersion, confirming that the dominant part of the scatter in the Hipparcos distances is caused by the trigonometric parallax errors and not by a large intrinsic dispersion of individual stellar distances. The distribution of secular parallaxes for Upper Sco is not resolved, which means that the distance spread cannot be larger than ~ 50 pc. Hence in the following we can assume that the Upper Sco association has a roughly spherical shape, i.e. that the intrinsic spread of distances is $\sim \pm(15-20)$ pc from the mean value of 145 pc.

Previous investigations of the IMF of Upper Sco based on the high-mass stellar content were carried out by de Geus et al. (1989) and Brown (1998). Using Walraven multi-color photometry, de Geus et al. (1989) established the membership of stars in Upper Sco and also determined their physical parameters ($\log g$ and $\log T_{\rm eff}$). From the latter one can determine the masses of the stars. Brown (1998) used the preliminary results on membership from the Hipparcos data to determine the luminosity function for the high-mass stars using the Hipparcos parallaxes, and then transformed a smoothed version of this into a mass function using the mass-luminosity relation listed in Miller & Scalo (1979). Adopting a conservative completeness limit of $V \approx 7$, which corresponds to masses of about 2.8 $M_\odot$, he concluded that down to this mass limit the IMF is consistent with a single power-law $\mathrm{d}N/\mathrm{d}M \propto M^\alpha$ with slope $\alpha \approx -2.9$. There are, however, several problems with this determination of the IMF, most importantly the fact that a mass-luminosity relation had been used that might not be appropriate for young stars (see discussion in Brown 1998).

Finally, Hoogerwerf (2000) attempted to extend the completeness of the kinematic studies of the membership of Upper Sco toward lower masses by making use of the TRC and ACT astrometric catalogs (Høg et al. 1998; Kuzmin et al. 1999; Urban et al. 1998), which are believed to be complete to $V \approx 10.5$. He selected some 250 candidate members with $V \approx 7-11$ from these catalogs by searching for stars with proper motions consistent with those of the Hipparcos association members, and which lie ≤ 1 mag below and ≤ 1.5 mag above the main sequence in the color-magnitude diagram. However, we note that the second selection criterion actually excludes most of the late-type association members[1], which, at an age of about 5 Myr, lie well above the main sequence (see Fig. 1). Therefore, and because no adequate spectroscopic and/or photometric information is available for most of these stars, we decided not to take this study into account.

2.2. Previous results on the low-mass population

Several searches for low-mass stars have been conducted in Upper Sco (e.g. Walter et al. 1994; Meyer et al. 1993; Sciortino et al. 1998; Martin et al. 1998; Ardila et al. 2000; for a summary see Preibisch, Guenther, & Zinnecker 2001, P01 hereafter). The first step in our own investigation of Upper Sco was a spectroscopic survey for PMS stars among ROSAT All Sky Survey (RASS) X-ray sources in a 160 square-degree area (Preibisch et al. 1998; P98 hereafter). In this spatially complete, but flux-limited survey covering nearly the full area of the association we found 39 new PMS stars. In Preibisch & Zinnecker (1999; PZ99 hereafter) we investigated the star formation history in Upper Sco. In a detailed analysis of the HR diagram, properly taking into account the uncertainties and the effects of unresolved binaries, we found that the low-mass PMS stars have a mean age of about 5 Myr and show no evidence for a large age dispersion. The PMS sample of PZ99 is statistically complete for stellar masses in the range from $\sim 0.8\,M_{\odot}$ to $\sim 2\,M_{\odot}$.

3. The 2dF survey for low-mass PMS stars

3.1. Aim of the survey and initial observations

The aim of the study presented here was to reveal the full population of low- and very-low mass ($\sim 0.1-0.8\,M_{\odot}$) stars in a representative area of Upper Sco. In combination with earlier studies this should allow a direct determination of the full IMF of this OB association. In order to reach this aim, it is essential that the search (1) is *unbiased*, i.e. *not* based on any pre-selection (e.g. X-ray selection), (2) allows a *reliable classification of the PMS nature* of the stars (which we achieved by measuring the strength of the 6708 Å Lithium line), and (3) covers a *large and representative area* of the association in order to yield a statistically meaningful sample (> 100 objects). A more detailed discussion of these aspects can be found in P01. Obviously, the only way to reach these goals is by obtaining spectra for many hundreds of stars, i.e. to perform a large multi-object spectroscopic survey.

Our first 2dF observations were performed in May 2000. The results are reported in Preibisch et al. (2001; P01 hereafter). We obtained spectra of 576 stars in two fields in Upper Sco, which we call 2dF-W and 2dF-E. Among these objects we were able to identify 98 new PMS stars, nearly all of them M-type stars, by their strong lithium absorption lines. As a large fraction of our observing time in May 2000 was lost due to bad weather, we re-applied for, and were awarded two more nights in May 2001.

3.2. New 2dF observations and data analysis

The data were obtained on the nights of May 16–17, 2001 with the 2dF instrument on the Anglo-Australian Telescope (AAT). 2dF is a fibre-fed multi-object spectrograph at the prime focus of the AAT that allows one to take spectra of up to 400 objects in a 2.1° diameter field. A full description of 2dF can be found at `http://www.aao.gov.au/2df/index.html`, and also in the recent paper by Lewis et al. (2002). P01 contains further details of our previous 2dF observations, similar to those being discussed here.

3.2.1. Field Configurations

In 2000 only field 2dF-W could be observed completely; in field 2dF-E spectra could be obtained only for the bright target stars. In the May 2001 observations we obtained spectra for the faint targets in 2dF-E and we observed faint as well as bright targets in a third field, which we will call 2dF-S. We originally planned to observe a fourth field, but due to cloudy periods in our observing

[1]A cross correlation between the kinematic candidate member list of Hoogerwerf (2000) and our list of PMS stars found in the 2dF survey shows no common objects.

nights we were not able to obtain any data for that field.

Positions and magnitudes of the target stars were obtained from scans of the R and I plates of the UKST survey fields 515, 516, and 584, measured for us with SuperCOSMOS, the Royal Observatory Edinburgh's high-precision microdensitometer (see Hambly et al. 1998). The SuperCOSMOS positions are good to better than $0.5''$, sufficient for 2dF spectroscopy. The transformation of the instrumental magnitudes to standard photometric magnitudes was done as described in PZ99. As for our previous observations, to maximize efficiency and to avoid problems with scattered light, we split each field into bright and faint subsamples. The bright sub-sample contains stars with $R = 12-15$, while the faint sub-sample extends from $R \sim 14-18$. The overlap between the two samples ($R = 14-15$) allows a useful check of the consistency of our line-width and spectral type measurements. The 2dF `Configure` program was used to allocate fibres to stars. We were able to allocate 104 and 80 fibres to target stars for the bright sub-samples in Fields 2dF-S and 2dF-E respectively, and 247 and 264 fibres to candidates for the faint sub-samples in these two fields; thus, a total of ~700 spectra were obtained. In addition, we also allocated fibres to 18 previously known PMS stars, which we observed with the aim of using them as spectral templates. Guide (fiducial) stars were also assigned, taken from our SuperCOSMOS star lists, for use in field acquisition and guiding. Finally, we allocated 80–100 fibres in each field to 'blank' sky regions for the bright configurations, and $\sim$ 60 sky fibres for the faint configurations. These fibres are used to form a mean sky spectrum, which is then subtracted from each of the program objects.

3.2.2. Observations and Data Reduction

We used the 1200R gratings in both spectrographs, with a central wavelength of 6700 Å, giving spectral coverage between 6150–7250 Å with a dispersion of 1.1 Å/pixel and a resolution of $\sim$ 2 Å. The sequence of observations was: tungsten flat (for mapping the spectra on the detector), CuAr + CuHe arc (for wavelength calibration), a series of object exposures, another arc, followed by $3\times$ 300 sec 'offset sky' exposures (where the telescope is offset from the field; these are used to calibrate the fibre-to-fibre throughputs). We obtained a total exposure of 1 hour for the 'bright' configurations in Fields 2dF-S and 2dF-E (split into 6×600 sec), and $\sim$ 5000 sec (split into 3 separate exposures) for the 'faint' configurations in these two fields. Telescope and weather problems prevented us from obtaining longer exposures for the faint configurations in these fields. Aside from some clouds in the second half of each night, observing conditions were good with seeing typically $1.6'' - 1.8''$. Field acquisition was straightforward, with confirmation of the reliability of our astrometry from the good registration of all 4 fiducial/guide stars on the guiding TV camera.

Data reduction was done using the standard `2dfdr` reduction package. `2dfdr` carries out preprocessing (bias-correction and trimming), flatfielding, tram-line mapping of the spectra on the CCD, subtraction of scattered light, optimal (weighted) spectral extraction, wavelength calibration, fibre throughput calibration, and sky subtraction. Our data reduction followed that of the 2dF Galaxy Redshift Survey (2dFGRS; see Colless et al. 2001), with the following changes. When working in the red part of the spectrum as we were, with many night sky lines, `2dfdr` gives one the option of using two methods for fibre throughput calibration: offset sky frames, or the strength of night sky lines. The 2dFGRS default is to use night sky line throughput calibration, but for our data better sky subtraction was obtained using the offset sky frames. We also turned off scattered light subtraction and did not flatfield our data, as these were introducing spurious features into our spectra. Spectra for the separate exposures for each field were combined *after* extraction; `2dfdr` allows this combining to be done in a robust manner, which accounts for different flux levels in the individual spectra (caused either by varying conditions or by different exposure times). The final, combined spectra have good sky subtraction and high S/N with a mean ranging between 70–90 for the bright configurations, and 50–70 for the faint configurations. Figure 3 in P01 shows some example spectra. We did not attempt to flux calibrate our spectra, which is always difficult to do with fibre spectroscopy.

3.2.3. *Spectral Analysis*

In total, we have obtained 592 usable spectra of 469 individual stars, including the 18 spectral templates stars. We used the IRAF[2] task *SPLOT* to determine the equivalent width of the 6708 Å Li line in all spectra. Most of our spectra are of sufficient quality to allow the unambiguous detection of the Li line with equivalent widths as low as $W \approx 0.04$ Å. In order to get a homogeneous data set we consider as 'Li-rich stars' all objects for which we find a Li equivalent width $W \gtrsim 0.1$ Å. Among the 469 previously unobserved stars for which we obtained spectra, 68 can be classified as Li-rich.

Our total 2dF data sample now consists of 1221 usable spectra for 1045 individual stars, among which we could identify 166 new Li-rich stars. For all Li-rich stars we determined the spectral type. This was done by comparison with our 2dF spectra of the 18 spectral template stars (previously known Upper Sco PMS stars from the lists of Walter et al. 1994, Köhler et al. 2000, Martin et al. 1998, and Ardila et al. 2000), covering a range of spectral types from K5 to M6. As described in P01, we employed a set of flux ratios over small wavelength ranges that are known to correlate with the spectral type and determined the 'best fit' relation between the spectral types of the template stars and the weighted mean of these relations. Our final 'best fit' relation was found to have a rms scatter of only 0.3 subtypes and was then used to compute spectral types for all our target spectra. We also compared the overall appearance of the target spectra against the grid of spectral templates and generally found very good agreement. We therefore assume our spectral types to be accurate to about 0.3 subclasses in nearly all cases. Due to the larger number of spectral templates and also the wider range of spectral types covered by the templates, our new spectral calibration is significantly better than that used in P01 for the 2000 data. We therefore re-determined the spectral types of the stars from the 2000 sample, which resulted in small changes of typically $\lesssim 0.2$ spectral subtypes, in a few cases up to 0.5 spectral subtypes.

For the classification as pre-main sequence (PMS) stars we adopted the spectral type dependent threshold for the 6708 Å Li line width as described in P98. All Li-rich stars in our 2dF sample lie above the PMS-threshold and therefore can be reliably classified as PMS stars. All but 5 of our Li-rich stars show the Hα line in emission; this is another indication for the youth of these objects. A list of all PMS stars detected in our 2dF survey (including the 2000 data as well as the 2001 data) is given in Table 1.

3.3. Results from the 2dF survey

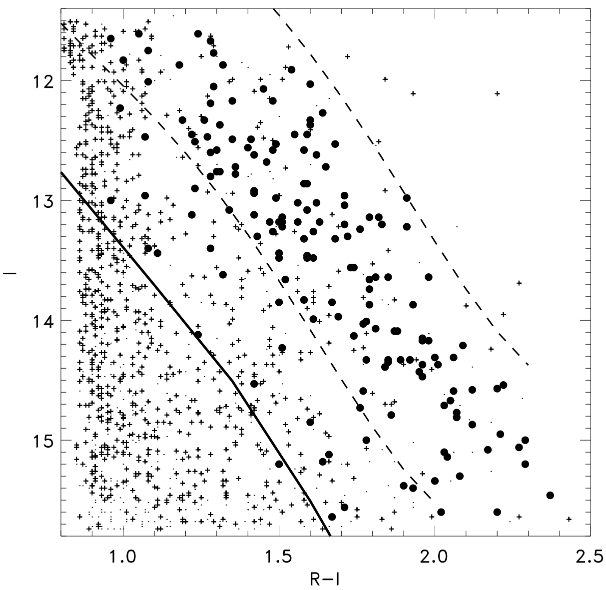

Fig. 1.— Color-Magnitude diagram for the targets of our 2dF survey. All objects in our target lists are shown as small dots. Stars that were observed with 2dF are shown as small crosses, and the Li-rich stars found with 2dF are shown as solid dots. The solid line shows the main sequence from Leggett (1992), the two dashed lines show the extension of the band defined by the previously known PMS stars in Upper Sco from PZ99.

In Fig. 1 we show the color-magnitude diagram of our targets. Nearly all objects which were classified as PMS stars spectroscopically by the strength of their Li absorption lines lie well above[3] the main

[2]IRAF is distributed by the National Optical Astronomy Observatories, which are operated by the Association of Universities for Research in Astronomy, Inc., under cooperative agreement with the National Science Foundation.

[3]Note that most of the few objects very close to the main

sequence, confirming their PMS status. The vast majority of the Li-rich stars lie within the band for primary photometric PMS candidates.

Our 2dF survey revealed 166 new PMS stars in an area in which only 26 PMS stars were previously known (PZ99). This means that our survey increased the known number of PMS stars in this area by a factor of more than 6. Figure 2 shows the spatial distribution of the new PMS stars with respect to the previously known low-mass PMS stars (PZ99) and the Hipparcos high-mass members (Z99).

3.4. The new HR diagram for the low-mass stellar population

In PZ99 and P01 we placed the PMS stars into the HR diagram and compared their locations with the D'Antona & Mazzitelli (1994) PMS models. In the upper part of Fig. 3 we show an updated HR diagram, where we have included the new PMS stars. We used the procedure as described in PZ99 to determine the extinctions, luminosities, and temperatures of the stars. For the M-type stars we used the 'intermediate temperature' scale defined by Luhman (1999), which has been shown to be most compatible with recent PMS models. The new HR diagram shows that the PMS stars detected with 2dF share the same locations as those identified in our earlier observations. A detailed discussion of the HR diagram of the previously known PMS stars in Upper Sco has been presented in PZ99. There we determined the mean age of the low-mass population by modeling its distribution in the HR diagram with a procedure that properly takes into account the observational uncertainties caused by photometric errors, the spread of individual stellar distances, and the effects of unresolved binaries. This statistical method predicts a band in the HR diagram for the expected locations of the PMS stars, given an assumed mean age and age spread. In Fig. 3 we have included the theoretical band of expected locations for a mean age of 5 Myr and no age spread, i.e. the age distribution as suggested by PZ99. The theoretical expectation that 90% of the stars should lie within this band if the assumed age distribution is correct, is very well confirmed by our data: 149 of the 166 PMS stars discovered with 2dF,

sequence suffer from a relatively high extinction.

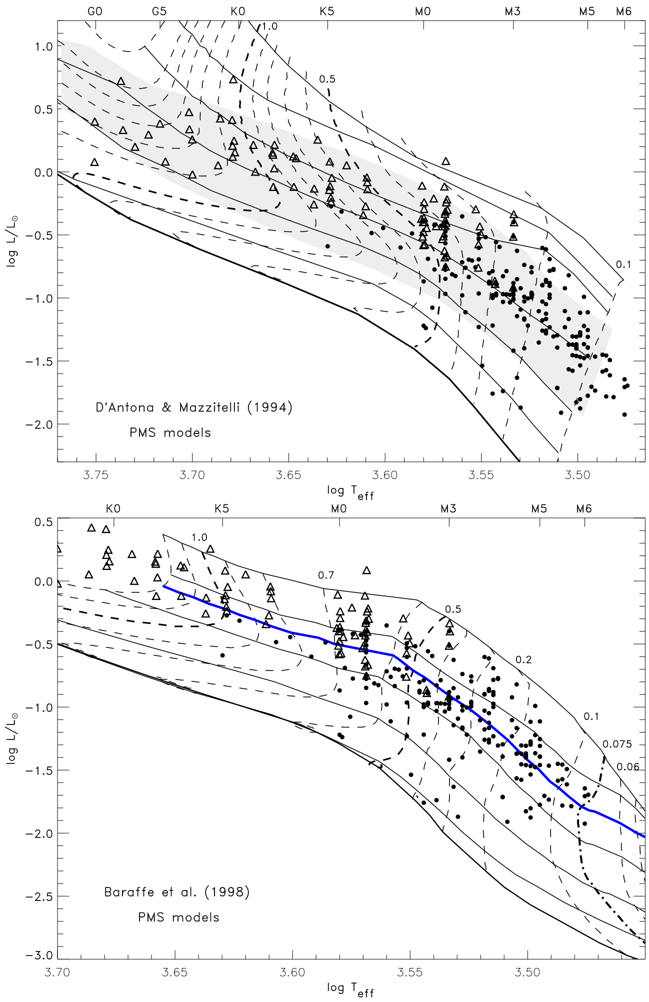

Fig. 3.— HR diagram for the PMS stars in Upper Sco, showing the previously known PMS stars from PZ99 as triangles while the new PMS stars detected with 2dF are shown as solid dots. The upper plot shows the evolutionary tracks (dashed lines) and isochrones (solid lines) from the D'Antona & Mazzitelli (1994) PMS models. The $1\,M_\odot$ and $0.5\,M_\odot$ track are shown as thick dashed lines. Isochrones are shown for ages of 0.1, 0.3, 1, 3, 10, and 30 Myr and finally the main sequence. The grey shaded band shows the region in which we expect 90% of the PMS stars to lie, based on the assumption of a common age of 5 Myr for all stars and properly taking into account the uncertainties and the effects of unresolved binaries (for details see text). The lower plot shows the evolutionary tracks (dashed lines) and isochrones (solid lines) from the Baraffe et al. (1998) PMS models. The $0.075\,M_\odot$ track is shown as thick dashed-dotted line. Isochrones are shown for the ages of 1, 3, 5, 10, 30, and 100 Myr and finally the main sequence. The 5 Myr isochrone is shown as the thick solid line.

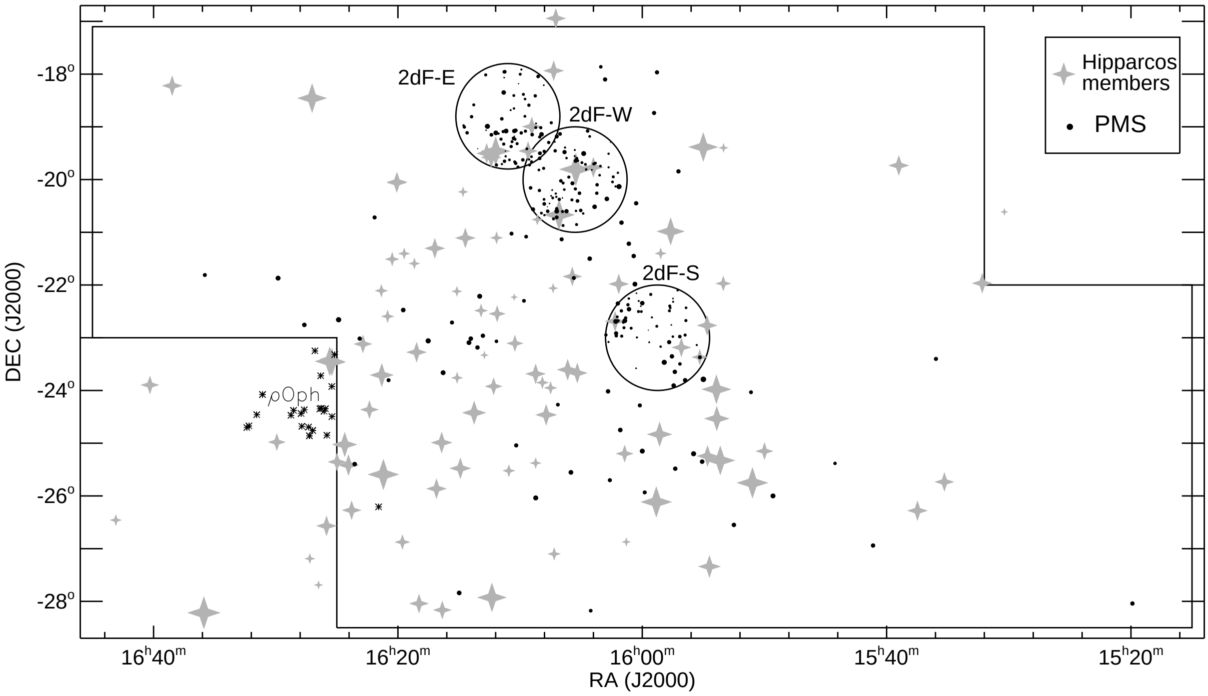

Fig. 2.— Map of the Upper Sco region. The 160 square-degree area of our previous X-ray survey (P98) is marked by the thick solid line. Our three 2dF fields are marked by circles. Hipparcos members are shown as asterisks and low-mass PMS stars as dots, with symbol size proportional to the magnitude of the stars. We also plot the T Tauri stars associated with the ρ Oph star forming region listed in the Herbig-Bell Catalogue (Herbig & Bell 1988) as small asterisks.

i.e. 89.8%, are located within the band. Our data are therefore fully consistent with a mean age of about 5 Myr and there is no evidence for a large age dispersion.

A potential reservation to this result comes from the uncertainties and ambiguities of the theoretical PMS models. The last few years, however, have brought considerable progress in the field of theoretical PMS models. It is now possible to use observational constraints, such as dynamical masses in multiple systems, to check the validity of different models. The models of Baraffe et al. (1998) have been found to be very consistent with observational constraints (see Luhman 1999; White et al. 1999). We therefore decided to also use the most recent version of the Baraffe et al. (1998) models, to investigate the ages and masses of the stars. These models start at an age of 1 Myr and cover masses from $0.02\,M_{\odot}$ up to $1.2\,M_{\odot}$. The lower plot in Figure 3 shows the HR diagram for the Upper Sco PMS stars compared with these models. Again, the general shape of the distribution of the stars follows the 5 Myr isochrone, fully confirming our earlier conclusions on the stellar ages.

We also employed the Baraffe et al. (1998) models to estimate the masses of the individual stars. The latest type (spectral type around M6) members are located very close to the stellar/substellar boundary at $0.075\,M_{\odot}$. Some of these objects might actually be young brown dwarfs; however, due to the uncertainties of our spectral calibration at these very cool temperatures we cannot make a very reliable assessment of their masses. In any case, it is clear that our survey includes several very-low-mass stars ($M \lesssim 0.1\,M_{\odot}$) and perhaps some brown dwarf candidates ($M \lesssim 0.075\,M_{\odot}$).

4. Properties of the high-mass members

For a careful study of the population of high-mass members it is important to know down to which mass the sample of Hipparcos members is complete. For stars earlier than G5 the Hipparcos completeness limit is given by Turon et al. (1992) as: $V \leq 7.9 + 1.1 \sin|b|$, where the Galactic longitude $|b|$ varies between ~ 15 and ~ 25 degrees for the bulk of the Upper Sco stars. This translates to a limiting magnitude out to which the sample is complete of $V \sim 8.2$–8.4. We adopt here a limit of $V = 8.2$, which corresponds to a limit in absolute magnitude of $M_V \approx 2$, or a limit in mass of ~ 2 $M_\odot$. The complete Hipparcos sample contains 62 A and B stars. Furthermore, there are 21 fainter A- and B-type Hipparcos members and 31 Hipparcos members of later spectral type. The A and B stars of Upper Sco have already evolved beyond their pre-main sequence phase and therefore 'standard' stellar evolutionary models can be used to determine their masses. For the F and G stars we need to take their PMS nature into account.

Our investigation of the high-mass stars is based on the list of Hipparcos members of Upper Sco (Z99) that contains 120 stars. Six of these stars are F/G/K giants; given the age of Upper Sco one would not expect these stars to be members and they are probably field star interlopers (see Z99 for an analysis of the expected number of field stars masquerading as association members). We will not consider them here. This leaves us with 114 Hipparcos members, for which we determined luminosities and masses, as explained below.

4.1. The color-magnitude diagram of the A and B stars

In deriving the color-magnitude diagram we do not take into account the effects of possible (close) binary companions. We will only determine the masses and luminosities of the primaries based on colors and magnitudes that have been corrected for extinction. We will also neglect the effects of stellar rotation and the subtle errors that may be introduced by using parallaxes to calculate the absolute magnitudes of the stars (although this will be much less of a problem when using the more precise secular parallaxes from de Bruijne 1999; see the discussion in Brown 1998).

The color magnitude diagram in the Johnson system (M_V vs. $(B-V)_0$) is derived from the data in table A1 in de Bruijne (1999). We calculated the absolute magnitudes from the so-called 'secular' parallaxes ($\pi_{\rm sec}$) in this table. These are the parallaxes derived from a careful kinematical modeling of the Hipparcos data for the Sco OB2 association and they are more precise than the original Hipparcos parallaxes. The values of $\pi_{\rm sec}$ used here correspond to the case $g_{\rm lim} = 9$ if available and to $g_{\rm lim} = \infty$ otherwise (see de Bruijne 1999). The value of the extinction A_V is taken from table A1 in de Bruijne (1999) where available. The values in that table were derived from either Walraven or Strömgren multi-color photometry. For stars without such photometry we used the value of $(B-V)$ and the relation between spectral type and $(B-V)_0$ to derive $E(B-V)$ and thus A_V. The calibrations of spectral type that were used were

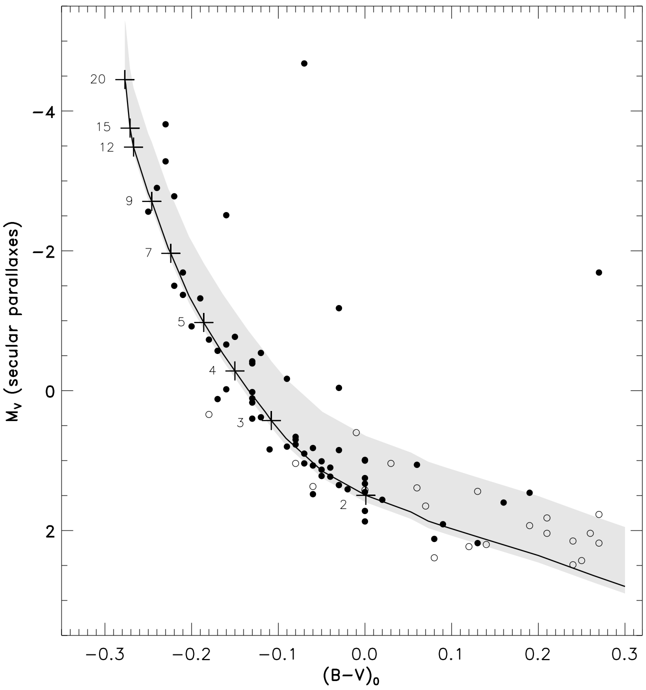

Fig. 4.— Color-magnitude diagram for the A- and B-type Hipparcos members of Upper Sco. The filled circles indicate the stars brighter than the Hipparcos completeness limit ($V \approx 8.2$), the open circles show the fainter stars. The 5 Myr isochrone is shown as the solid line. The labeled crosses mark stellar masses between $2\,M_\odot$ and $20\,M_\odot$ on the isochrone. The grey band shows the width of the corresponding binary sequence plus a ± 0.1 mag band to account for distance- and photometric errors.

those in table A5 of Kenyon & Hartmann (1995) for dwarfs and those of Schmidt–Kaler (1982) for the giants and super-giants. Keep in mind that using this method for determining $E(B-V)$, assumes main sequence colors for the stars. The resulting color-magnitude diagram is shown in Fig. 4 together with a 5 Myr isochrone. This isochrone is a combination of the isochrones for intermediate mass stars by Girardi et al. (2000) and for high mass stars as used in Bertelli et al. (1994) based on Bressan et al. (1993)[4].

As stated above no correction was applied for the effects of binary stars in the color-magnitude diagram. This causes a spread in the sequence of stars in both color and magnitude. Some of the conspicuous outliers are stars with peculiarities (see also de Bruijne 1999) and the M1Ib+B2.5V star HIP 80763 (Antares) is not visible in this diagram although it is a member of Upper Sco.

4.2. Masses of the A and B stars

De Zeeuw & Brand (1985) and de Geus et al. (1989) independently investigated the ages of the B- and A-stars in Upper Sco. Both studies derived an age of $5-6$ Myr from the main sequence turnoff in the HR diagram. Another estimate was obtained kinematically, by tracing back the motions of the stars until the smallest configuration is reached; this yielded an age of ~ 5 Myr (Blaauw 1991), in full agreement with the nuclear ages. As noted by de Geus et al. (1989), there is no evidence for a significant spread in ages among the high-mass stars.

As can be seen from Fig. 4 the color-magnitude diagram for the Hipparcos members is indeed consistent with all the stars having an age of 5 Myr. Hence, their masses are determined from their locations in the color-magnitude diagram using the 5 Myr isochrone as follows. For each star the Euclidean distance to each isochrone point is calculated and the minimum value of this distance then corresponds to the point on the isochrone where the initial mass of the star is read off. Simple linear interpolation is used to calculate 1000 points on the isochrones between 1 and 20 Solar masses. For the 5 Myr isochrone this range of masses maps uniquely to M_V and $(B-V)_0$. Using this method the value of the mass is mainly determined by the absolute magnitude of the star and not so much by its color. The reason for this becomes clear when examining Fig. 4 from which one can see that the magnitude scale is roughly 10 times larger than the color scale. Hence M_V is much more sensitive to the initial mass. For the outliers in the color-magnitude diagram (HIP 78207, 80112, 81474) we determined their masses by assigning the median mass at that spectral type.

The masses determined in this way for the A and B stars range from $1.7\,M_\odot$ up to $16.8\,M_\odot$ for the B0.5V star HIP 78820 (HD 144217). In addition, there are two even more massive cluster members. One is the the M1Ib Supergiant HIP 80763, i.e. Antares. As this star is already at a late stage of evolution, we estimate its initial mass by comparison with stellar evolution models to be about $M \sim 20-25\,\mathrm{M}_\odot$. A more accurate estimate is hardly possible, because these models sensitively depend on factors such as stellar rotation, core overshoot, and the mass-loss history (see Meynet & Maeder 2000 and references therein). Furthermore, it is most likely that Upper Sco once contained an even more massive star, that already exploded as a supernova about 1 Myr ago. Evidence for this comes from the existence of the runaway star ζ Oph (Blaauw 1961), the initial mass function and the age of Upper Sco (Blaauw 1991, de Geus 1992), and the observed kinematics of a large expanding HI shell surrounding Upper Sco (see Blaauw 1991; de Geus 1992 and references therein). This has recently been confirmed nicely through a detailed study of OB runaway stars by Hoogerwerf et al. (2000) (see Hoogerwerf et al. 2001). By carefully tracing back the motions of ζ Oph and the pulsar PSR J1932+1059 Hoogerwerf et al. (2000) showed that both stars were located in the same location 1 Myr ago and thus very likely formed a binary in which the pulsar progenitor exploded as a Supernova, thereby releasing ζ Oph as a runaway O star. Hence for a Supernova explosion ~ 1 Myr ago, i.e. at a stellar age of ~ 4 Myr, the pulsar progenitor must have had a mass of $\sim 40-60\,M_\odot$. For its former companion, the runaway star ζ Oph, we estimate a mass of $\sim 20\,M_\odot$ from its O9 spectral type.

[4] These isochrones have been transformed to several different photometric systems as described in Girardi et al. (2000). The tables can be retrieved from `http://pleiadi.pd.astro.it`

5. The full stellar population of Upper Sco

The combination of the different studies of Upper Sco yields a sample of 364 association members and finally allows a detailed investigation of the full stellar population of this OB association. The sample of the 114 Hipparcos members covers the full extent of the association and provides a complete sample of all individual member stars with masses above $2\,M_\odot$ and an (incomplete) sample of lower-mass members with masses down to $\sim 1\,M_\odot$. The 166 low-mass PMS stars identified with 2dF constitute a statistically complete, unbiased sample of the member population in the ~ 0.1–$0.8\,M_\odot$ mass range, which covers a 9 square-degree area. The 84 X-ray selected PMS stars from PZ99 provide a statistically complete sample of the $\sim 0.8 - 2 M_\odot$ members (plus some lower mass stars) in a 160 square-degree area.

5.1. The HR-diagram and the age of the full stellar population

In Fig. 5 we present an HR diagram containing all Upper Sco association members from the samples defined above. For the Hipparcos members we have determined the effective temperatures and luminosities from the $B-V$ colors and M_V magnitudes using the relations listed in Kenyon & Hartmann (1995). The diagram also shows the main sequence and a 5 Myr isochrone. One can see that not only the majority of the low-mass stars, but also most of the intermediate- and high-mass stars lie close to or on the 5 Myr isochrone. The apparent deviations can be explained by spectral peculiarities, binarity, observational uncertainties and the distance spread. It is also remarkable that this isochronal age is very well consistent with previous and absolutely independent determinations based on the nuclear and kinematic ages of the massive stars (de Zeeuw & Brand 1985; de Geus et al. 1989), which also yielded 5 Myr. This very good agreement of the *independent* age determinations for the high-mass and the low-mass stellar population shows that *low- and high-mass stars are coeval* and thus have formed together. Furthermore, the absence of a significant age dispersion implies that all stars in the association have formed more or less simultaneously. This means that the star-formation process must have started rather suddenly and everywhere at the same time in the association, and also must have ended rather suddenly after at most a few Myr. The star formation process in Upper Sco can thus be considered as a *burst of star formation*. This will be discussed in more detail in Section 6.

5.2. The initial mass function over the full stellar mass range $(0.1 - 20\,M_\odot)$

Our large sample of Upper Sco members provides a very good opportunity for a detailed look at the mass function. To determine the mass function in the 0.1–20 $M_\odot$ mass range, we have counted the number of stars in certain mass bins. For the 2dF sample and the later-type stars in the X-ray selected sample we used the Baraffe et al. (1998) models and a bin size of $0.1\,M_\odot$ for masses below $1\,M_\odot$. For the earlier-type stars in the X-ray selected sample (which are not covered by the Baraffe models) and for the F- and G-type Hipparcos members we used the Palla & Stahler (1999) models (which agree well with the Baraffe models near $1\,M_\odot$); in the mass range from $1\,M_\odot$ to $3\,M_\odot$ a bin size of $0.5\,M_\odot$ was used. For the B- and A-type Hipparcos members we used the mass estimates determined in section 4 and a bin size of $1\,M_\odot$ for masses above $3\,M_\odot$.

Before we can combine our three samples into a single mass function, we have to take into account that only the Hipparcos sample is fully complete and covers the full extent of the association. For the 2dF sample and the X-ray selected sample we have to correct for observational completeness and spatial coverage. In our 2dF survey we have obtained useable spectra for 86% of the photometric candidates in the survey area (see P01). The fraction of stars observed is generally independent of their magnitudes, but among the faintest target ($R \gtrsim 17$) the fraction of objects that yielded spectra with insufficient S/N is somewhat larger than among the brighter targets. Taking this into account, we find that the observational completness of our 2dF sample is 87% for stars with masses above $0.2\,M_\odot$, and 67% for stars with masses in the range $0.1 - 0.2\,M_\odot$. Our 2dF survey covered an area of 9 square-degrees; the spatial extrapolation factor relating this survey area to the full association can be determined in the following way: The smallest rectangular area including all three 2dF fields has a size of $5° \times 6°$ and contains 38 of the 114 Hipparcos members. Assuming that the

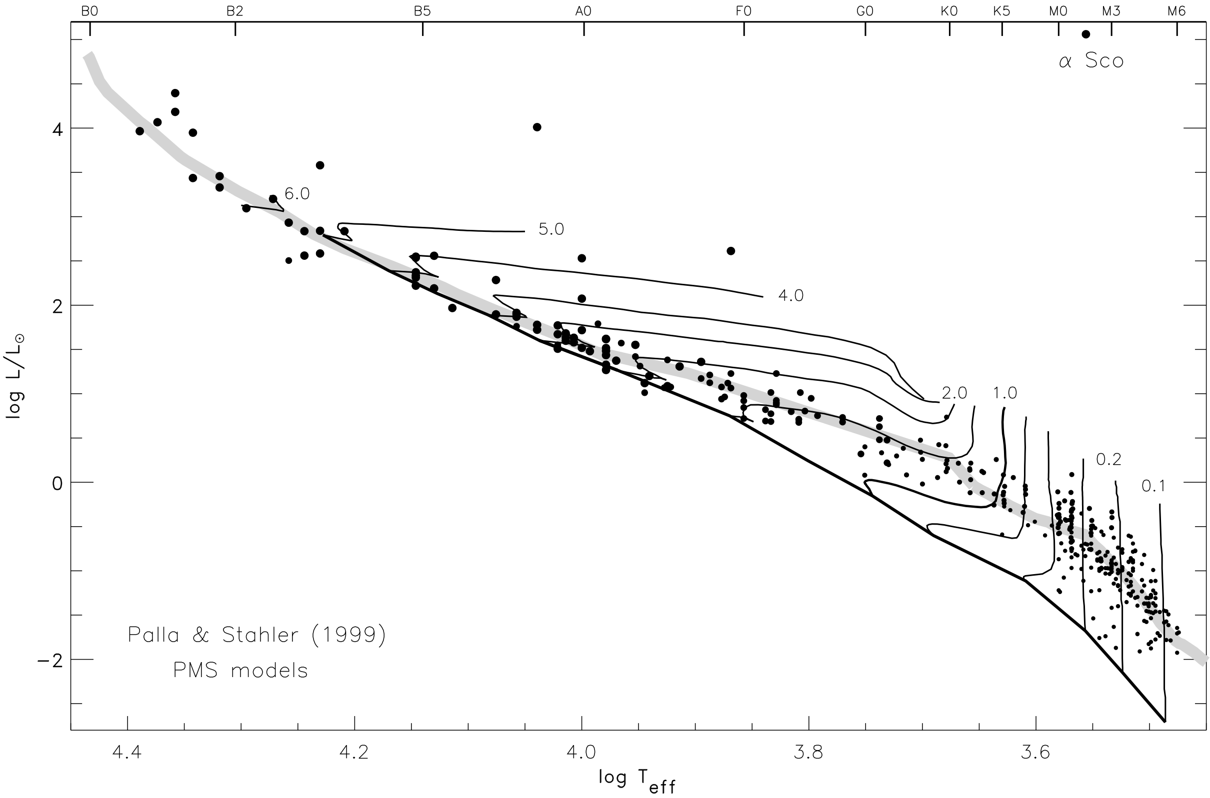

Fig. 5.— HR diagram for the Upper Sco association members in the Hipparcos sample, the X-ray selected sample and the 2dF sample. The lines show the evolutionary tracks from the Palla & Stahler (1999) PMS models, some labeled by their masses in solar units. The thick solid line shows the main sequence. The 5 Myr isochrone is shown as the thick grey line; it was composed from the high-mass isochrone from Bertelli et al. (1994) for masses $6-30\,M_{\odot}$, the Palla & Stahler (1999) PMS models for masses $1-6\,M_{\odot}$, and the Baraffe et al. (1998) PMS models for masses $0.02-1\,M_{\odot}$.

populations of low- and high-mass members share the same spatial distribution (as found in PZ99), it follows that this 30 square-degree area includes 34.6% of the stellar population. Therefore, the full extrapolation factor to be used for the 2dF sample is $\frac{100}{87} \times \frac{30}{9} \times \frac{114}{38} = 11.49$. For the $0.1{-}0.2\,M_{\odot}$ bin the factor is 14.92.

The completeness of the X-ray selected sample has been estimated to be about 75% (PZ99) for objects with masses above $\sim 0.8\,M_{\odot}$. In our spectroscopic survey (P98) 65% of the X-ray selected candidates were observed, and the area of that survey included 85 of the 114 Hipparcos members. Therefore, the extrapolation factor is $\frac{100}{75} \times \frac{100}{65} \times \frac{114}{85} = 2.75$

Finally, we mention that we have not (and cannot) considered the effects of binarity for the stellar masses. Our mass function therefore represents the *primary star mass function*. Therefore, ζ Oph is not included as it was originally the binary companion of the supernove progenitor. Figure 6 shows the histogram representation of our empirical mass function. The contribution from each of the three subsamples is multiplied by the corresponding extrapolation factor.

Before we consider the detailed shape of the mass function, we note that building a histogram is the simplest, but by no means optimum way of analysing the distribution of masses. One of the problems related to histograms is that an unfavorable choice of the bin size can easily lead to artificial features: too small a bin size can for example

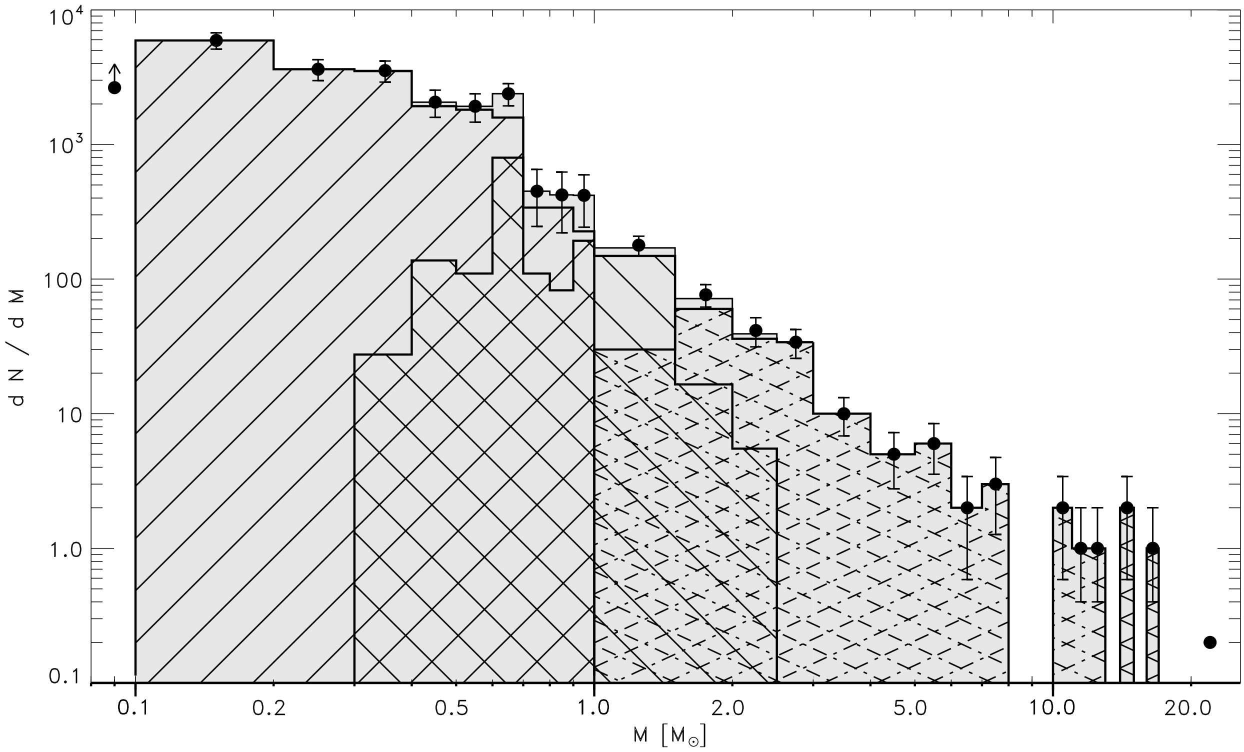

Fig. 6.— The emipirical mass function of the Upper Sco OB association in the $0.1 - 20\,M_\odot$ range. The left hatched histogram shows the 2dF sample, the central hatched histogram shows the X-ray sample, and the right double-hatched histogram shows the Hipparcos sample. The solid dots and the grey filled area mark the sum of the individual samples. The dot at $22.5\,M_\odot$ represents Antares.

cause spikes in the histogram; if, however, the bin size is too large, the inherent local structure of the distribution is lost. Despite these disadvantages, we are forced to use histograms because our mass function is composed of three subsamples with different extrapolation factors, and there is no better way to combine different sub-samples. In order to avoid loss of valid information, we choose a relatively small bin size. A potential problem caused by this can be seen in the $0.6 - 0.7\,M_\odot$ mass bin, which shows a local peak, whereas one would expect a smooth decline. Given the intrinsic uncertainties in our spectral type determination that translate into corresponding mass-uncertainties, it is obvious that some of the objects in this bin might actually have masses slightly outside the bin range. In order to avoid artificial features and to properly take into account the precision of our mass estimates, we 'smoothed' our histogram by folding it with an adaptive kernel function in the following way: Consider the bin i centered at mass M_i and with bin size ΔM. The temperature error originating from the uncertainty in the spectral type determination in that part of the HR diagram corresponds to a certain mass error $\sigma(M_i)$. Then, the fraction $f_i = \frac{\sigma(M_i)}{\Delta M}$ of the objects in bin $i-1$ as well as bin $i+1$ might also be assigned to bin i. A smooth estimate $\widetilde{N_i}$ of the number of objects in bin i can then be computed by

$$\widetilde{N_i} = \frac{1}{1 + 2\,f_i}\,(N_i + f_i\,N_{i-1} + f_i\,N_{i+1}) \ . \qquad (1)$$

For the case of mass errors equal to the bin size, i.e. $\sigma(M_i) = \Delta M_i$ or $f_i = 1$, this expression corresponds to a simple boxcar average of width 3 bins. For the binning scheme we have used to build our histogram, the quantity f_i ranges from ~ 0.3 to ~ 1.

Figure 7 shows the smoothed representation of the mass function in Upper Sco. It is immediately

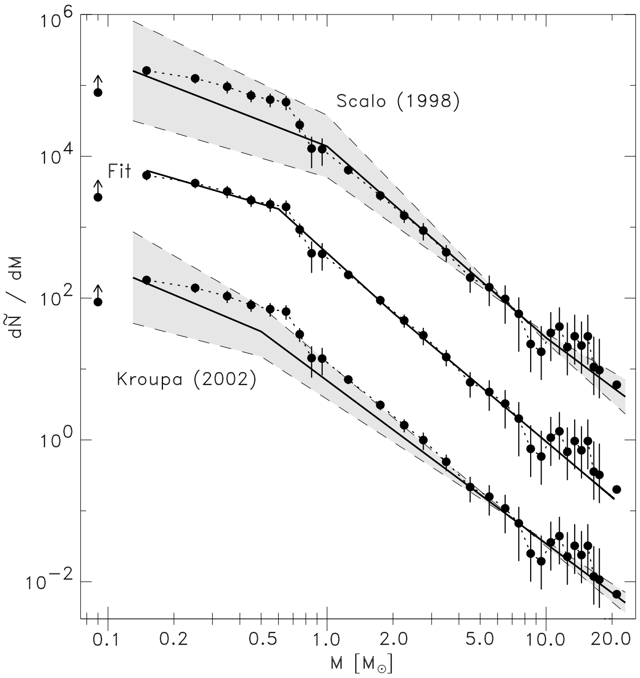

Fig. 7.— Comparison of our smoothed mass function for the Upper Sco association with different models. The Upper Sco mass function is shown three times by the solid dots connected by the dotted lines, multiplied by arbitrary factors. The middle curve shows the original mass function, the solid line is our multi-part power-law fit. The upper curve shows our mass function multiplied by a factor of 30 and compared to the Scalo (1998) IMF (solid line); the grey shaded area delimited by the dashed lines represents the range allowed by the errors of the model. The lower curve shows our mass function multiplied by a factor of 1/30 and compared to the Kroupa (2002) IMF (solid line).

apparent that the mass function cannot be reproduced by a single power law, because the slope in the low-mass part $(0.1-0.8\,M_\odot)$ is much flatter than in the intermediate- and high-mass range. To describe the detailed shape of the mass function, we will use multi-part power law functions for the probability density distribution of the form $\mathrm{d}N/\mathrm{d}M \propto M^\alpha$. In the $0.1-20\,M_\odot$ range our mass function is very well described by the following function:

$$\frac{\mathrm{d}N}{\mathrm{d}M} \propto \begin{cases} M^{-0.9\pm0.2} & \text{for} \quad 0.1 \le M/M_\odot < 0.6 \\ M^{-2.8\pm0.5} & \text{for} \quad 0.6 \le M/M_\odot < 2 \\ M^{-2.6\pm0.5} & \text{for} \quad 2 \le M/M_\odot < 20 \end{cases} \tag{2}$$

or, in shorter notation, $\alpha[0.1-0.6] = -0.9 \pm 0.2$, $\alpha[0.6-2.0] = -2.8 \pm 0.5$, $\alpha[2.0-20] = -2.6 \pm 0.3$.

We now compare our mass function to different IMF models. First, we consider the IMF as suggested by Scalo (1998), which is given by $\alpha[0.1-1] = -1.2 \pm 0.3$, $\alpha[1-10] = -2.7 \pm 0.5$, $\alpha[10-100] = -2.3 \pm 0.5$. In Fig. 7 we compare this model to our data. The normalization of the model curve was obtained by requiring a match with the observed mass function in the $7-8\,M_\odot$ bin. The comparison shows that the Scalo (1998) IMF reproduces the observed mass function above $1\,M_\odot$ quite well; below $1\,M_\odot$, however, the agreement gets worse: we clearly find more stars in the $0.2-0.7\,M_\odot$ range than expected from the model. Another important discrepancy is that our mass function flattens at $\sim 0.6\,M_\odot$, not at $1\,M_\odot$ as predicted by the Scalo (1998) IMF. In general, however, if we take into account the intrinsic uncertainties of the model IMF, our mass function is consistent with the Scalo (1998) IMF.

Kroupa (2002) summarized recent IMF determinations and suggested the following parametrization for the average galactic field star IMF in the solar neighborhood: $\alpha[0.02-0.08] = -0.3 \pm 0.7$, $\alpha[0.08–0.5] = -1.3 \pm 0.5$, $\alpha[0.5–100] = -2.3 \pm 0.3$. This model is compared to our mass function in Fig. 7. It does not well reproduce the shape of the Upper Sco mass function below $\sim 4\,M_\odot$; the deviations appear to be even larger than in the comparison to the Scalo (1998) IMF. However, the Kroupa (2002) model predicts the flattening to occur at $0.5\,M_\odot$, similar to what we find in our mass function.

While the slopes of our best-fit mass function are generally different from those of the Scalo

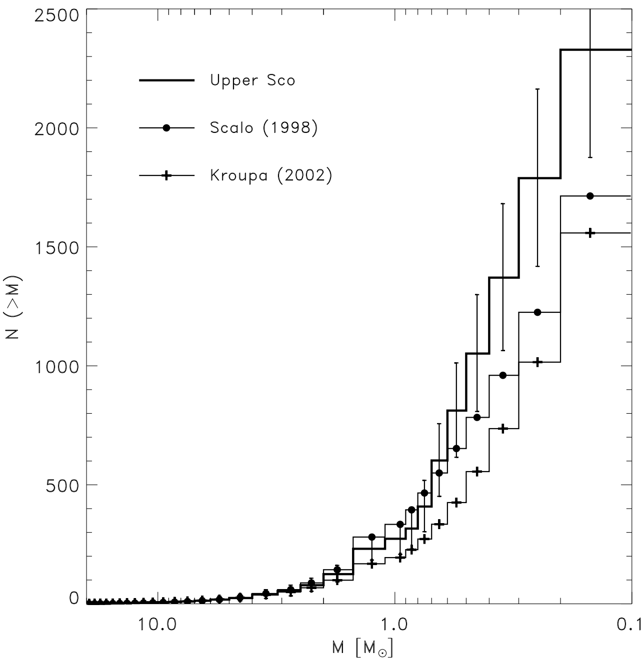

Fig. 8.— This figure shows the cumulative initial mass function of the Upper Sco OB association as a histogram. The Scalo (1998) IMF is shown by the solid dots, the Kroupa (2002) IMF by the crosses.

(1998) and Kroupa (2002) IMFs, we note that they are well within the ranges of slopes derived for similar mass ranges in other young clusters or associations, as compiled in Kroupa (2002). Therefore, we conclude that, within the uncertainties, the general shape of our mass function is consistent with recent field star and cluster IMF determinations.

Nevertheless, there is a noticeable difference when comparing the cumulative mass function of our sample to the field star IMF predictions. The comparison in Fig. 8 shows that Upper Sco contains more low-mass stars than expected from the field IMF. The comparison to the Scalo (1998) IMF suggests an excess of $\sim$ 560 stars in the 0.1–0.7 $M_\odot$ range. The comparison to the Kroupa (2002) IMF suggests an excess of $\sim$ 760 stars in the $0.1 - 2.0\,M_\odot$ range. However, we note that the statistical significance of this excess is below the '2σ level', and therefore not fully convincing. However, our results make it clear that *there is certainly no deficit of low-mass stars in Upper Sco.*

6. The Star Formation Process in Upper Sco

Upper Sco is an ideal place to study *the outcome of recent star formation.* As the active star formation phase is finished, the observed distribution of stellar masses and ages represents the final result of the star formation process. All young stars are optically visible since the parental molecular cloud is nearly fully dispersed.

6.1. Basic characteristics

The *stellar population* in the $0.1\,M_\odot$ to $20\,M_\odot$ mass range can be described by our 'best fit' mass function (eqn. 2). The integration of this function yields 2525 stars with a total mass of $1400\,M_\odot$. 75% of all stars have masses below $0.6\,M_\odot$ and contribute 39% of the total mass. Only 3% of all stars have masses above $2\,M_\odot$, but they contribute 33% of the total mass. All these numbers are based on the primary star mass function. For a reasonable estimate of the total stellar mass we have to take into account that most of the stars are probably in multiple systems. The binary frequency (i.e. the probability that a given object is multiple; cf. Reipurth & Zinnecker 1993) for late type stars is at least about 50% (c.f. Duquennoy & Mayor 1991; Fischer & Marcy 1992; see Köhler et al. 2000 for the case of Upper Sco) and even higher for early type stars (Mason et al. 1998; Abt et al. 1990; Preibisch et al. 1999). We can estimate the total mass of the companions in the multiple systems as follows: assuming a binary frequency of 100% and random pairing of secondaries from the same underlying mass function (eqn.2) as the primaries, we find that the total mass of all companions in the $0.1 - 20\,M_\odot$ mass range is 40% of the total mass of all primaries. For the estimate of the total stellar mass we also have to include the most massive stars: Antares ($\sim 22\,M_\odot$) and its B2.5 companion ($\sim 8\,M_\odot$), the supernova progenitor ($\sim 50\,M_\odot$), and ζ Oph ($\sim 20\,M_\odot$). The total stellar mass is then : $1.4 \times 1400\,M_\odot + 22\,M_\odot + 8\,M_\odot + 50\,M_\odot + 20\,M_\odot = 2060\,M_\odot$.

The *star formation efficiency* can be estimated in the following way: De Geus (1992) determined the mass of the HI shell surrounding Upper Sco to be $\sim 80\,000\,M_\odot$. Using this value as an estimate for the original cloud mass, the star formation efficiency is $\sim 2060\,M_\odot/80\,000\,M_\odot \sim 2.6\%$. This value is in the typical range of star formation efficiencies in many molecular clouds (see Cohen & Kuhi 1979) and suggests that only a very small fraction of the initial cloud mass was transformed into stars.

We now turn to the *star formation history* and deal with the question of how the star formation process proceeded in Upper Sco. A very important aspect here is the spatial extent of the association. The bulk (70%) of the Hipparcos members (and thus also the low-mass stars) lie within an area of 11 degrees diameter on the sky, which implies a characteristic size of the association of 28 pc. De Bruijne (1999) showed that the internal velocity dispersion of the Hipparcos members of Upper Sco is only 1.3 km/s. From these numbers, the initial size of the association can be estimated in the following way: We assume that the association was immediately unbound after a short gas expulsion phase (caused by the numerous massive stars; see below) and that the stars expanded freely from their initial positions. Assuming a Gaussian velocity distribution characterized by the measured velocity dispersion, a single point in space would have expanded to a size of about 13 pc in 5 Myr. Subtracting this number from the current characteristic size of 28 pc in quadrature leads to an initial size of 25 pc. This implies a lateral crossing time of 25 pc / 1.3 km s^{-1} $\sim$ 20 Myr. This large period of time is in remarkable contrast to the age spread of the association members: as we found above, neither the high-mass stars nor the low-mass stars show any evidence for a significant age spread and our data are consistent with the idea that all stars have formed within a period of not more than $\sim 1-2$ Myr. Therefore, it is obvious that the lateral crossing time is much (about an order of magnitude) larger than the age spread of the association members. This finding clearly shows that some external agent is required to have coordinated the onset of the star formation process over the full spatial extent of the association. In order to account for the small spread of stellar ages, the triggering agent must have crossed the initial cloud with a velocity of at least $\sim 15-25$ km/s. Finally, some mechanism must have terminated the star formation process at most about 1 Myr after it started. We believe that both effects were caused by massive stars.

6.2. The impact of the massive stars

Massive stars, above about ten solar masses, profoundly affect their environment in several ways. The strong ionizing radiation of O-type stars can photoevaporate molecular cloud clumps (e.g. see Hester et al. 1996 and McCaughrean & Andersen 2002 for the case of M16) and circumstellar matter around young stellar objects (see Bally et al. 1998; Richling & Yorke 1998; 2000). Their powerful stellar winds deposit considerable amounts of momentum and kinetic energy into the surrounding medium. For example, a single O5 star is perfectly capable of dispersing a $10^4\,M_\odot$ molecular cloud completely within only about 1 Myr (see Yorke 1986). Finally, supernova explosions cause strong shock waves that transfer typically some 10^{51} erg of kinetic energy into the ambient interstellar medium. The supernova blast wave will initially expand within the wind-blown bubble formed by the supernova progenitor; as it catches up with the bubble shock front, it will accelerate the expansion of the bubble (see e.g. Oey & Massey 1995) and further disrupt the parental molecular cloud (see e.g. Yorke et al. 1989).

In general, massive stars have a very destructive effect on their nearby environment; they can disrupt molecular clouds very quickly and therefore prevent further star formation in their surroundings. At somewhat larger distances, however, the wind- and supernova-driven shock waves originating from massive stars can have a constructive rather than destructive effect by driving molecular cloud cores into collapse. Several recent numerical studies (e.g. Boss 1995; Foster & Boss 1996, 1997; Vanhala & Cameron 1998; Fukuda & Hanawa 2000) have found that the outcome of the impact of a shock wave on a cloud core mainly depends on the type of the shock and its velocity: In its initial, adiabatic phase, the shock wave is likely to destroy ambient clouds; the later, isothermal phase, however, is capable of triggering cloud collapse if the velocity is in the right range. Shocks traveling faster than about 50 km/s shred cloud cores to pieces, while shocks with velocities slower than about 15 km/s usually cause only a slight temporary compression of cloud cores. Shock waves with velocities in the range of $\sim 15-45$ km/s, however, seem to be well able to induce collapse of molecular cloud cores. A good source of shock waves with velocities in that range are supernova explosions at a distance[5] between $\sim$ 10 pc and $\sim$ 100 pc. Other potential sources of such shock waves include wind-blown bubbles and expanding HII regions. Observational evidence for star forming events triggered by shock waves from massive stars has for example been discussed in Carpenter et al. (2000), Walborn et al. (1999), Yamaguchi et al. (2001), Efremov & Elmegreen (1998), and Oey & Massey (1995).

6.3. Triggered star formation in Upper Sco

For the star burst in Upper Sco, a very suitable trigger is a supernova explosion in the Upper Centaurus-Lupus association that happened about 12 Myr ago. The structure and kinematics of the large H I loops surrounding the Scorpius-Centaurus association suggest that this shock wave passed through the former Upper Sco molecular cloud just about 5–6 Myr ago (de Geus 1992). This point in time agrees very well with the ages found for the low-mass stars as well as the high-mass stars in Upper Sco, which have been determined above in an absolutely independent way. Furthermore, since the distance from Upper Centaurus-Lupus to Upper Sco is about 75 pc, this shock wave probably had precisely the properties ($v \sim 20-25$ km/s) that are required to induce star formation according to the modeling results mentioned above. Thus, the assumption that this supernova shock wave triggered the star formation process in Upper Sco provides a self-consistent explanation of all observational data.

The shock-wave crossing Upper Sco initiated the formation of some 2500 stars, including 10 massive stars upwards of $10\,M_{\odot}$. When the newborn massive stars 'turned on', they immediately started to destroy the cloud from inside by their ionizing radiation and their strong winds. This affected the cloud so strongly that after a period of $\lesssim$ 1 Myr the star formation process was terminated, probably simply because all the remaining dense cloud material was disrupted. This explains the narrow age distribution and why only about 2% of the original cloud mass was transformed into stars. About 1.5 Myr ago the most massive star in Upper Sco, the progenitor of the pulsar PSR J1932+1059, exploded as a supernova. This explosion led to the ejection of its companion star as the runaway star ζ Oph (see Hoogerwerf et al. 2001) and created a strong shock wave, which fully dispersed the Upper Sco molecular cloud and removed basically all the remaining diffuse material.

It is interesting to note that this shock wave must have crossed the ρ Oph cloud within the last 1 Myr (de Geus 1992). The strong star formation activity we witness right now in the ρ Oph cloud might therefore be triggered by this shock wave (see Motte et al. 1998) and would represent the third generation of sequential triggered star formation in the Scorpius-Centaurus-Ophiuchus complex.

7. Summary and conclusions

Our 2dF survey reveals 166 new low-mass PMS stars in a 9 square-degree area in Upper Sco. Their distribution in the HR diagram suggests that the new low-mass stars show the same rather narrow age distribution around 5 Myr that we had previously derived for a smaller sample of Upper Sco members. We determine luminosities and masses for the Hipparcos members of Upper Sco and create an HR diagram for the full stellar population, ranging from $0.1\,M_{\odot}$ up to $20\,M_{\odot}$. We find that stars of all masses have a common age of 5 Myr. This confirms our previous suggestion that the star formation process in Upper Sco can be characterized as a super-nova triggered mini-starburst.

We have determined the shape of the complete stellar mass function in Upper Sco. The slopes of our mass function are consistent with those of recent field star IMF determinations within the uncertainties. We find some evidence for an excess of low-mass stars, which however is significant at the 2σ level only. Nevertheless, our data clearly prove that there is no lack of low-mass stars in this OB association.

Further progress is possible in several ways. An obvious aim would be to extend the search for association members to even lower masses, i.e. into

[5] Generally, if the supernova is too close, the shock wave will be too fast and destroy the core, whereas if the supernova is too far away the shock wave will be too slow to trigger collapse. The exact values of the suitable distance obviously depend on the details of the processes creating the shock wave (see Oey & Massey 1995), the structure of the surrounding medium, and the evolutionary state of the pre-impact core.

the sub-stellar regime. The photometric search for member candidates by Ardila et al. (2000) revealed an excess of brown dwarf candidates over the number predicted by the Miller-Scalo initial mass function. This result is in good qualitative agreement with our finding of an excess of very low-mass stars and makes a spectroscopic survey for brown dwarfs very promising.

Another significant improvement can be gained by a better characterization of the multiplicity of the association members. Literature data on multiplicity is available for the Hipparcos members and a subset of the lower mass members. This data is however highly affected by numerous selection effects that have not been studied so far (see Brown 2001). We will tackle this problem by supplementing the available literature data (radial velocity surveys, Hipparcos data, existing adaptive optics and speckle data, etc) with newly obtained adaptive optics observations of stars in Sco OB2. We also note that due to its declination and the exceptionally well known member population, Upper Sco is an ideal target for ESO's VLTI to perform an interferometric survey for very close binary systems. On the other hand state of the art numerical simulations will be used to perform detailed calculations of the evolution of OB associations, including the detailed evolution of the binary stars. The results will be used to generate simulated observations that can be compared to the actual data, leading to a much more complete understanding of the properties of the binary population of Sco OB2 (see Brown, 2001, for more details). The distribution of binary frequencies and mass ratios as a function of spectral type will be obtained, which can then be used to make a comprehensive and final study of the IMF of Upper Scorpius including the effects of multiplicity.

We thank the referee, Tim de Zeeuw, for his very prompt report and his constructive criticism, which helped to improve the paper. We also would like to thank the SuperCOSMOS Group at the Royal Observatory Edinburgh for scanning the UKST plates for us and Thomas Blöcker for advice on estimating masses of evolved stars.

REFERENCES

Abt H.A., Gomez A.E., Levy S.G., 1990, ApJS 74,551
D'Antona, F., Mazzitelli, I., 1994, A&AS 90, 467
Ardila D., Martin E., Basri G., 2000, AJ 120,479
Bally, J., Sutherland, R.S., Devine, D., Johnstone, D. 1998, AJ 116, 293
Baraffe I., Chabrier G., Allard F., Hauschildt P.H., 1998, A&A 337,403
Bertelli G., Bressan A., Chiosi C., Fagotto F., Nasi E., 1994, A&AS, 106, 275
Blaauw A., 1961, Bull. Astr. Inst. Neth., 15, 265
Blaauw A., 1991, In: Lada C.J., Kylafis N.D. (eds.) The Physics of Star Formation and Early Stellar Evolution, NATO ASI Vol. 342, p. 125
Boss, A.P. 1995, ApJ 439, 224
Bressan A., Fagotto F., Bertelli G., Chiosi C., 1993, A&AS, 100, 647
Brown A.G.A., 1998, In: The Stellar Initial Mass Function, eds. G. Gilmore, D. Howell, ASP Conf Ser. Vol. 142, p. 45
Brown A.G.A., 2001, Astron. Nachr. 322, 43
de Bruijne J.H.J., 1999, MNRAS 310,585
Carpenter J.M., Heyer M.H., Snell R.L, 2000, ApJS 130,381
Cohen M., Kuhi L.V., 1979, ApJS 41,743
Colless M., Dalton G., Maddox S., et al., 2001, MNRAS, 329, 87
Dolan C.J., Mathieu R.D., 2001, AJ 121,2124
Duquennoy A., Mayor M., 1991, A&A 248,485
Efremov Y.N., Elmegreen B.G., 1998, MNRAS 299,643
Fischer D.A., Marcy G.W., 1992, ApJ 396,178
Foster, P.N., & Boss, A.P. 1996, ApJ 468, 784
Foster, P.N., & Boss, A.P. 1997, ApJ 489, 346
Fukuda, N., & Hanawa, T. 2000, ApJ 533, 911
de Geus E.J., 1992, A&A 262,258
de Geus, E.J., de Zeeuw, P.T. & Lub, J., 1989, A&A 216, 44
Girardi L., Bressan A., Bertelli G., Chiosi C., 2000, A&AS 141, 371
Hambly N.C., Miller L., MacGillivray H.T., Herd J.T., Cormack W.A., 1998, MNRAS 298,897
Hester J.J., Scowen P.A., Sankrit R., et al., 1996, AJ 111,2349
Herbig G.H., 1962, Adv. Astron. Astrophys., 1,47
Herbig G.H., Bell K.R., 1988, Lick Observatory Bulletin No. 1111
Høg, E., Kuzmin, A., Bastian, U., et al. 1998, A&A, 335, L65
Hoogerwerf, R. 2000, MNRAS, 313, 43
Hoogerwerf, R., de Bruijne, J.H.J., de Zeeuw, P.T. 2000, ApJ, 544, L133
Hoogerwerf, R., de Bruijne, J.H.J., de Zeeuw, P.T. 2001, A&A, 365, 49
Kenyon S.J., Hartmann L., 1995, ApJS, 101, 117
Köhler R., Kunkel M., Leinert C. Zinnecker H., 2000, A&A 356,541
Kroupa P., 2002, Science, Vol. 295, No. 5552, p. 82
Kuzmin, A., Høg, E., Bastian, U., et al. 1999, A&AS, 136, 491
Larson R.B., 1986, MNRAS 218,409

Legett S.K., 1992, ApJS 82,351

Leitherer C., 1998, In: The Stellar Initial Mass Function, eds. G. Gilmore, D. Howell, ASP Conf Ser. Vol. 142, p. 61

Lewis I.J., Cannon R.D., Taylor K., et al., 2002, MNRAS, in press (astro-ph/0202175)

Luhman K.L., 1999, ApJ 525,466

Martin E.L., Montmerle T., Gregorio-Hetem J., Casanova S., 1998, MNRAS 300,733

Mason B.D., Gies D.R., Hartkopf W.I., et al., 1998, AJ 115,821

Meyer M.R., Wilking B.A., Zinnecker H., 1993, AJ 105,619

Meynet G., Maeder A., 2000, A&A 361,101

McCaughrean M.J., Andersen M., 2002, A&A, in press

Miller G.E., Scalo J.M., 1979, ApJS 41,513

Motte F., André P., Neri R., 1998, A&A 336,150

Oey, M.S. & Massey, P. 1995, ApJ, 452, 210

Palla F., Stahler S.W., 1999, ApJ 525,772

Preibisch Th., Zinnecker H., 1999, AJ 117,2381 (PZ99)

Preibisch Th., Guenther E., Zinnecker H., Sterzik M., Frink S., Röser S., 1998, A&A 333,619 (P98)

Preibisch Th., Balega Y., Hofmann K.-H., Weigelt G., Zinnecker H., 1999, New Astronomy 4, 531

Preibisch Th., Guenther E., Zinnecker H., 2001, AJ 121,1040 (P01)

Reipurth B., Zinnecker H., 1993, A&A 278,81

Richling, S. & Yorke, H.W. ,1998, A&A 340, 508

Richling, S. & Yorke, H.W., 2000, ApJ 539,258

Scalo J.M., 1998, In: Gilmore G., Howel D. (eds.) The stellar intial mass function, ASP Conference Series Vol. 142, p. 201

Schmidt–Kaler Th., 1982, in Landolt–Börnstein New Series, Group VI, Vol. 2b, p. 1, eds K. Schaifers & H.H. Voigt (Springer–Verlag)

Sciortino S., Damiani F., Favata F., Micela G., 1998, A&A 332,825

Shu F.H., Lizano S., 1988, In: Stellar Matter, Moran J.M., Ho P.T.P. (eds.), Gordon & Breach, p. 65

Turon C., et al., 1992, Hipparcos Input Catalogue, ESA SP–1136

Urban, S.E., Corbin, T.E., Wycoff, G.L. 1998, AJ, 115, 2161

Vanhala, H. A. T & Cameron, A. G. W. 1998, ApJ 508, 291

Walborn N.R., Barba R.H., Brandner W., Rubio M., Grebel E.K., Probst R.G., 1999, AJ 117,225

Walter, F.M., Vrba, F.J., Mathieu, R.D., Brown, A., & Myers, P.C., 1994, AJ 107,692

White R.J., Ghez A.M., Reid I.N., Schultz G., 1999, ApJ 520,811

Wilking B.A., 1991, In: Reipurth B. (ed.) Low Mass Star Formation in Southern Molecular Clouds, ESO Scientific Report No. 11, p. 159

Yamaguchi R., Mizuno N., Onishi T., Mizuno A., Fukui Y., 2001, ApJ 553,L185

Yorke, H.W. 1986, ARAA, 24, 49

Yorke, H.W., Tenorio-Tagle, G., Bodenheimer, P., Rozyczka, M. 1989, A&A 216, 207

de Zeeuw P.T., Brand J., 1985, In: van den Woerden H., Boland W. (eds.) Birth and Evolution of Massive Stars and Stellar Groups, Reidel, Dordrecht, p. 95

de Zeeuw P.T., Hoogerwerf R., de Bruijne J.H.J., Brown A.G.A., Blaauw A., 1999, AJ 117,354

Zinnecker H., McCaughrean M.J., Wilking B.A., 1993, In: Levy E.H., Lumine J.I. (eds.) Protostars and Planets III, University of Arizona Press, p. 429

This 2-column preprint was prepared with the AAS LATEX macros v5.0.

TABLE 1

PMS STARS IN UPPER SCO DETECTED IN OUR 2DF SURVEY. THE SOURCE NAME IN THE FIRST COLUMN CONSISTS OF THE J2000 COORDINATES OF THE STAR. THE FOLLOWING COLUMNS GIVE THE R-BAND MAGNITUDE, THE EQUIVALENT WIDTH OF THE 6708Å LI LINE AND THE Hα LINE, THE SPECTRAL TYPE, THE EXTINCTION, THE ADOPTED EFFECTIVE TEMPERATURE AND THE BOLOMETRIC LUMINOSITY.

(6) Source USco-	(7) R [mag]	(8) W(Li) [Å]	W(Hα) [Å]	SpT	A_V [mag]	$\log T_{\rm eff}$ [K]	$\log \frac{L}{L_\odot}$
155532.4-230817	16.8	0.15	0.5	M1	5.7	3.569	-0.75
155624.8-222555	15.5	0.78	-5.4	M4	1.7	3.516	-1.12
155625.7-224027	14.6	0.53	-4.2	M3	1.8	3.532	-0.85
155629.5-225657	14.3	0.54	-3.1	M3	0.9	3.533	-0.98
155655.5-225839	13.1	0.54	-1.9	M0	0.7	3.578	-0.69
155706.4-220606	16.2	0.52	-3.6	M4	2.0	3.513	-1.31
155728.5-221904	16.7	0.40	-6.2	M5	2.3	3.505	-1.37
155729.2-221523	17.1	0.29	-4.0	M5	2.1	3.503	-1.58
155729.9-225843	15.8	0.55	-7.0	M4	1.4	3.511	-1.30
155737.2-224524	16.7	0.15	0.0	M2	1.6	3.544	-1.76
155742.5-222605	15.7	0.15	-2.9	M3	1.8	3.526	-1.22
155744.9-222351	14.3	0.13	0.9	M2	0.7	3.558	-1.11
155746.6-222919	14.7	0.69	-2.1	M3	1.3	3.533	-1.01
155829.8-231007	15.4	0.41	-250.0	M3	0.0	3.532	-1.63
155848.6-224657	14.5	0.19	-0.5	M0	0.7	3.579	-1.24
155912.5-223650	16.4	0.89	-10.5	M5	0.3	3.493	-1.70
155918.4-221042	14.7	0.98	-1.0	M4	1.3	3.515	-0.90
155925.9-230508	17.0	0.65	-19.5	M6	1.5	3.485	-1.57
155930.1-225125	17.6	0.70	-5.0	M4	2.5	3.511	-1.71
160004.3-223014	14.9	0.20	-0.4	M3	0.2	3.528	-1.40
160007.2-222406	16.8	0.27	-4.4	M4	0.6	3.509	-1.91
160017.4-221810	16.5	0.50	-3.9	M6	0.0	3.481	-1.79
160018.4-223011	14.7	0.30	-150.0	M3	1.5	3.539	-0.97
160026.3-225941	16.8	1.00	-10.0	M5	2.5	3.495	-1.25
160028.5-220922	16.8	0.65	0.0	M6	0.0	3.476	-1.93
160030.2-233445	17.2	0.50	-15.8	M6	1.0	3.476	-1.71
160054.5-224908	14.7	0.10	0.0	M3	1.0	3.530	-1.09
160106.0-221524	15.9	0.80	-8.0	M5	1.0	3.501	-1.38
160110.4-222227	14.2	0.80	-9.4	M4	1.0	3.513	-0.78
160121.5-223726	14.2	0.80	-8.4	M4	0.4	3.507	-0.92
160129.8-224838	14.9	0.80	-4.4	M4	1.6	3.515	-0.90
160132.9-224231	14.6	0.20	-1.4	M0	0.9	3.580	-1.22
160140.8-225810	14.0	0.45	-120.0	M3	0.0	3.528	-1.16
160142.6-222923	13.5	0.33	-0.6	M0	0.7	3.580	-0.87
160158.9-224036	14.4	0.80	-7.6	M4	0.7	3.515	-0.97
160159.7-195219	16.3	0.47	-2.7	M5	2.0	3.497	-1.22
160202.9-223613	14.7	0.18	-1.5	M0	1.6	3.575	-1.08
160207.5-225746	13.7	0.30	-3.2	M1	0.9	3.565	-0.81
160210.9-200749	16.4	0.65	-3.5	M5	1.6	3.501	-1.40
160222.4-195653	14.7	0.40	-6.6	M3	1.6	3.533	-0.95
160226.2-200241	15.2	0.47	-4.9	M5	0.0	3.495	-1.39
160236.2-191732	17.3	0.40	0.7	M3	2.5	3.539	-1.74
160245.4-194604	15.9	0.30	0.7	M2	1.4	3.550	-1.54
160245.4-193037	16.4	0.51	-1.1	M5	1.8	3.495	-1.31
160245.7-230450	16.7	1.00	-100.0	M6	1.5	3.485	-1.46
160258.5-225649	13.9	1.00	-9.4	M2	0.8	3.546	-0.88
160325.6-194438	15.4	0.20	-1.4	M2	1.6	3.544	-1.22
160329.4-195503	15.7	0.40	-4.9	M5	1.0	3.503	-1.30
160341.8-200557	13.5	0.30	-2.2	M2	0.9	3.555	-0.70
160343.3-201531	13.6	0.49	-3.5	M2	0.9	3.558	-0.76
160350.4-194121	15.0	0.59	-4.9	M5	0.6	3.505	-1.17
160357.9-194210	14.5	0.35	-3.0	M2	1.7	3.546	-0.87
160407.7-194857	16.8	0.22	-4.0	M5	0.7	3.499	-1.80
160418.2-191055	15.4	0.76	-0.5	M4	2.3	3.524	-0.99
160428.0-190434	15.8	0.55	-3.4	M4	2.4	3.516	-1.05
160428.4-190441	13.5	0.68	-5.0	M3	1.0	3.532	-0.63
160435.6-194830	16.1	0.63	-7.2	M5	1.6	3.499	-1.29

Table 1—*Continued*

(6) Source USco-	(7) R [mag]	(8) W(Li) [Å]	W(Hα) [Å]	SpT	A_V [mag]	$\log T_{\rm eff}$ [K]	$\log \frac{L}{L_\odot}$
160439.1-194245	15.1	0.61	-3.8	M4	0.9	3.518	-1.18
160449.9-203835	16.0	0.65	-7.8	M5	1.0	3.497	-1.37
160456.4-194045	15.0	0.54	-5.2	M4	0.9	3.507	-1.10
160502.1-203507	13.6	0.57	-5.9	M2	1.8	3.551	-0.53
160508.3-201531	13.3	0.58	-4.3	M4	0.0	3.524	-0.80
160508.5-201532	14.0	0.46	-5.5	M4	0.4	3.518	-0.90
160516.1-193830	15.6	0.50	-2.4	M4	1.1	3.520	-1.35
160517.9-202420	12.9	0.41	-5.2	M3	0.6	3.542	-0.56
160521.9-193602	13.9	0.50	-1.9	M1	1.2	3.563	-0.83
160522.7-205111	14.8	0.10	-4.5	M4	1.1	3.518	-1.03
160525.5-203539	16.1	0.48	-6.1	M5	1.5	3.499	-1.30
160528.5-201037	14.1	0.55	-1.9	M1	1.4	3.569	-0.85
160531.3-192623	16.7	0.58	-8.8	M5	1.8	3.497	-1.48
160532.1-193315	16.5	0.61	-26.0	M5	0.0	3.499	-1.88
160545.4-202308	14.4	0.31	-35.0	M2	1.4	3.560	-0.98
160600.6-195711	14.9	0.80	-7.5	M5	1.7	3.505	-0.82
160611.9-193532	16.0	0.63	-8.2	M5	0.9	3.495	-1.39
160619.3-192332	16.4	0.52	-5.5	M5	1.9	3.505	-1.37
160622.8-201124	15.4	0.53	-6.0	M5	0.0	3.499	-1.47
160628.7-200357	15.0	0.58	-30.0	M5	0.6	3.499	-1.12
160629.0-205216	15.1	0.68	-6.2	M5	1.2	3.497	-0.99
160632.1-202053	17.3	0.69	-5.1	M5	1.5	3.495	-1.78
160643.8-190805	12.7	0.65	-3.8	K6	1.9	3.623	-0.31
160647.5-202232	13.9	0.41	-3.2	M2	1.6	3.557	-0.70
160700.1-203309	14.1	0.65	-0.6	M2	1.8	3.551	-0.69
160702.1-201938	16.3	0.39	-30.0	M5	1.7	3.501	-1.37
160704.7-201555	16.2	0.61	-4.2	M4	1.7	3.511	-1.39
160707.7-192715	14.0	0.57	-5.0	M2	2.2	3.548	-0.52
160708.7-192733	15.8	0.52	-4.0	M4	1.7	3.516	-1.26
160710.0-191703	16.6	0.90	-9.0	M2	3.6	3.551	-1.23
160716.0-204443	14.7	0.68	-3.6	M4	1.2	3.524	-0.97
160719.7-202055	15.3	0.57	-2.3	M3	2.7	3.542	-0.89
160722.4-201158	17.2	0.50	-14.0	M5	2.3	3.491	-1.47
160726.8-185521	14.1	0.33	-1.9	M1	1.1	3.569	-0.97
160727.5-201834	17.3	0.90	-13.0	M5	2.4	3.487	-1.45
160735.5-202713	17.2	0.75	-4.9	M5	2.3	3.505	-1.57
160739.4-191747	14.0	0.52	-2.3	M2	1.6	3.560	-0.72
160744.5-203602	13.6	0.50	-4.8	M4	0.8	3.516	-0.61
160745.8-203055	17.3	0.30	-2.0	M3	1.9	3.530	-1.87
160800.5-204028	16.3	0.34	-5.2	M5	1.9	3.501	-1.31
160801.4-202741	12.8	0.83	-2.3	K8	1.5	3.601	-0.45
160801.5-192757	14.0	0.52	-3.6	M4	1.0	3.524	-0.76
160802.4-202233	15.3	0.60	-6.1	M5	0.5	3.499	-1.27
160803.6-181237	17.3	0.35	-7.7	M4	3.9	3.515	-1.23
160804.3-194712	14.0	0.91	-5.2	M4	0.0	3.516	-1.17
160815.3-203811	15.1	0.57	-1.9	M3	2.1	3.542	-0.98
160818.4-190059	14.1	0.72	-3.7	M3	0.3	3.528	-1.03
160822.4-193004	12.9	0.29	-3.0	M1	1.2	3.571	-0.43
160823.2-193001	13.1	0.49	-6.0	K9	1.5	3.586	-0.49
160823.5-191131	14.1	0.59	-4.1	M2	1.5	3.544	-0.79
160823.8-193551	13.2	0.72	-2.1	M1	1.5	3.569	-0.47
160825.1-201224	13.7	0.41	-2.0	M1	1.3	3.574	-0.77
160827.5-194904	15.6	0.57	-12.3	M5	1.4	3.495	-1.11
160841.7-185610	16.9	0.70	-11.0	M6	1.1	3.483	-1.61
160843.1-190051	14.9	0.57	-5.8	M4	1.3	3.515	-1.00
160845.6-182443	13.7	0.70	0.5	M3	0.2	3.533	-0.93
160854.0-203417	14.8	0.57	-3.4	M4	1.5	3.518	-0.90

TABLE 1—*Continued*

(6) Source USco-	(7) R [mag]	(8) W(Li) [Å]	W(Hα) [Å]	SpT	A_V [mag]	$\log T_{\rm eff}$ [K]	$\log \frac{L}{L_\odot}$
160900.0-190836	15.9	0.62	-15.4	M5	0.7	3.503	-1.45
160900.7-190852	12.8	0.53	-12.7	K9	0.8	3.592	-0.60
160903.9-193944	14.6	0.68	-7.2	M4	0.6	3.520	-1.10
160904.0-193359	15.5	0.80	-2.2	M4	2.5	3.524	-0.96
160908.4-200928	13.4	0.66	-4.0	M4	0.7	3.518	-0.60
160913.4-194328	14.9	0.54	-1.6	M3	1.8	3.537	-0.97
160915.8-193706	16.1	0.78	-4.4	M5	0.7	3.499	-1.53
160916.8-183522	13.8	0.55	-3.0	M2	1.0	3.546	-0.80
160926.7-192502	14.9	0.40	0.0	M3	1.0	3.528	-1.16
160933.8-190456	14.1	0.57	-3.5	M2	1.4	3.557	-0.83
160935.6-182822	15.5	0.75	-4.2	M3	1.8	3.528	-1.17
160936.5-184800	15.0	0.57	-18.0	M3	1.2	3.532	-1.14
160943.8-182302	15.0	0.48	-5.8	M4	1.9	3.516	-0.86
160946.4-193735	13.5	0.49	-1.6	M1	1.6	3.569	-0.57
160953.6-175446	16.6	1.30	-22.0	M3	4.1	3.539	-1.03
160954.4-190654	13.5	0.70	-3.1	M1	0.9	3.569	-0.78
160959.4-180009	14.7	0.58	-4.0	M4	0.2	3.518	-1.26
161007.5-181056	17.8	0.44	-13.3	M6	1.9	3.474	-1.70
161010.4-194539	14.7	0.49	-5.6	M3	1.4	3.533	-1.01
161011.0-194603	16.2	0.70	-4.4	M5	0.3	3.487	-1.58
161014.7-191909	14.4	0.62	-2.3	M3	1.0	3.535	-0.97
161021.5-194132	14.0	0.40	-4.3	M3	2.0	3.541	-0.59
161024.7-191407	14.9	0.55	-3.7	M3	1.5	3.528	-0.99
161026.4-193950	15.0	0.62	-4.4	M4	1.9	3.516	-0.87
161028.1-191043	17.3	0.65	-11.4	M4	2.1	3.511	-1.72
161030.0-183906	16.1	0.54	-6.5	M4	2.0	3.507	-1.23
161030.9-182422	15.1	0.55	-3.4	M3	1.8	3.535	-1.04
161031.9-191305	12.6	0.50	-2.3	K7	1.1	3.607	-0.48
161039.5-191652	14.5	0.53	-4.3	M2	1.5	3.551	-0.96
161043.9-192225	14.0	0.67	-2.3	M3	1.1	3.539	-0.83
161046.3-184059	16.8	0.51	-7.2	M4	3.1	3.516	-1.28
161052.4-193734	15.4	0.93	-3.9	M3	2.3	3.526	-1.00
161110.9-193331	16.2	0.63	-6.3	M5	1.1	3.501	-1.46
161112.3-192737	17.3	0.30	-50.0	M5	1.4	3.501	-1.83
161115.3-175721	13.1	0.55	-2.4	M1	1.6	3.574	-0.42
161116.6-193910	13.9	0.47	-3.4	M4	0.6	3.513	-0.77
161118.1-175728	13.9	0.55	-4.8	M4	0.9	3.515	-0.69
161118.2-180358	17.5	0.90	-20.0	M6	1.6	3.476	-1.65
161120.4-191937	14.1	0.51	-5.5	M2	0.6	3.544	-1.00
161123.0-190522	14.4	0.40	-6.9	M3	1.7	3.528	-0.74
161129.4-194224	16.4	0.80	-13.0	M6	0.8	3.483	-1.49
161133.6-191400	14.4	0.56	-3.7	M3	1.8	3.537	-0.79
161146.1-190742	16.2	0.47	-6.3	M5	1.6	3.503	-1.37
161156.2-194323	14.1	0.60	-6.3	M3	0.7	3.542	-0.97
161247.2-190353	17.4	0.88	-10.6	M6	1.3	3.485	-1.78
161248.9-180052	14.6	0.52	-3.8	M3	1.4	3.530	-0.92
161328.0-192452	17.8	0.40	-17.0	M5	2.2	3.491	-1.73
161347.5-183459	14.6	0.52	-3.5	M2	1.5	3.544	-0.98
161358.1-184828	13.7	0.57	-1.9	M2	1.0	3.553	-0.76
161420.2-190648	13.2	0.37	-52.0	K5	1.8	3.630	-0.59
161433.6-190013	14.2	0.64	-26.0	M2	2.2	3.551	-0.60
161437.5-185823	15.7	0.13	-3.6	M3	1.4	3.533	-1.42

NOTE.—The following PMS stars can be identified with stars classified as candidate members of Upper Sco by Ardila et al. (2000): USco-155925.9-230508 = CTIO 67; 160026.3-225941 = CTIO 53; 160030.2-233445 = CTIO 75; 160245.7-230450 = CTIO 55.